Journal of Power Sources 253 (2014) 360–365

Contents lists available at ScienceDirect

Journal of Power Sources

journal homepage: www.elsevier.com/locate/jpowsour

Solid state synthesis of Fe_2P nanoparticles as high-performance anode materials for nickel-based rechargeable batteries

Yaping Wang [b], Lili Zhang [b], Huanhuan Li [c], Yijing Wang [a,*], Lifang Jiao [a], Huatang Yuan [a], Long Chen [c], Hua Tang [b], Xiaofei Yang [b]

[a] Institute of New Energy Material Chemistry, Key Laboratory of Advanced Energy Materials Chemistry (MOE), Collaborative Innovation Center of Chemical Science and Engineering (Tianjin), Tianjin Key Lab on Metal and Molecule-based Material Chemistry, Nankai University, Tianjin 300071, PR China
[b] School of Material Science & Engineering, Jiangsu University, Zhenjiang 212013, PR China
[c] Automotive Engineering Research Institute, Jiangsu University, Zhenjiang 212013, PR China

HIGHLIGHTS

- We report a new way to prepare Fe_2P nanoparticles for the first time.
- Fe_2P is firstly used as anode materials for nickel-based rechargeable batteries.
- The reversible discharge capacity of Fe_2P nanoparticles is about 413 mAh g^{-1}.
- Fe_2P nanoparticles exhibit attractive rate capability.

ARTICLE INFO

Article history:
Received 12 October 2013
Received in revised form
6 December 2013
Accepted 12 December 2013
Available online 19 December 2013

Keywords:
Nickel-based rechargeable battery
Anode material
Diiron phosphide nanoparticle
Solid state synthesis
Electrochemical property

ABSTRACT

Using a green and effective method based on the solid state reaction between $FePO_4 \cdot 2H_2O$ and KBH_4, high pure Fe_2P nanoparticles are successfully prepared. The mass ratio of $FePO_4 \cdot 2H_2O$ to KBH_4 has a decisive influence on the composition of the products. Moreover, Fe_2P nanoparticles exhibit considerably high discharge capacities and excellent rate capability as the anode materials for nickel-based rechargeable batteries. The reversible discharge capacities are 413 and 343 mAh g^{-1} at currents of 100 and 500 mA g^{-1}, respectively. It is expected that Fe_2P nanoparticles have potential applications in nickel-based rechargeable batteries.

1. Introduction

Climate change and exhaust of fossil fuels drive the worldwide interest in using electricity instead of internal combustion engines to propel vehicles. Thus far, batteries have been considered the most available devices for powering hybrid electric vehicles and all-electric vehicles. Nickel-based rechargeable batteries (i.e., Ni–Fe [1,2], Ni–Cd [3–5], Ni–MH [6–9] and Ni–Zn [10,11] batteries) are one of the most important power sources. For example, Ni–MH batteries are one of the most successful power supplies for hybrid electric vehicles in use today such as Toyota Prius. To meet the ever increasing requirements of the battery powered vehicles, current efforts are directed towards the development of new anode materials with higher capacities, better cycling performance and lower cost for nickel-based rechargeable batteries.

Recently, some transition metal–metalloid compounds have been found to exhibit promising anodic performance for nickel-based rechargeable batteries [12–17]. Among them, the cobalt-based materials such as cobalt borides [12–14] and cobalt phosphides [15,16] have received special attention for their high discharge capacities and excellent cycle stabilities. However, this type of material is always expensive owing to the use of cobalt or its compounds. As we all know, iron has similar properties to cobalt but is much cheaper. Therefore, the iron-based compounds such as iron borides are also evaluated as anode materials for nickel-based rechargeable batteries [13,17]. Although the

* Corresponding author. Tel./fax: +86 22 23503639.
E-mail address: wangyj@nankai.edu.cn (Y. Wang).

0378-7753/$ – see front matter © 2013 Elsevier B.V. All rights reserved.
http://dx.doi.org/10.1016/j.jpowsour.2013.12.056

discharge capacities of iron borides are competitive, their cycling performance is disappointing. This is possibly attributed to the poor anti-corrosive capability of iron boride electrodes in alkaline aqueous electrolyte [17].

We are interested in exploiting an iron-based anode material with relatively high discharge capacities and excellent cycling performance. Considering the better anti-corrosion property of phosphorus to boron in alkaline aqueous electrolyte, iron phosphides are highly desirable for nickel-based rechargeable batteries. However, current methods for preparing iron phosphides either require relatively high temperature/long reaction time, or use highly toxic reactants such as PH_3 or trioctylphosphine (TOP) [18–20]. Thus, the development of new routes facilitating the green and fast synthesis of iron phosphides at a relatively low temperature is of great interest.

Herein, we report a facile and green strategy to synthesize Fe_2P nanoparticles *via* the solid state reaction of $FePO_4{\cdot}2H_2O$ and KBH_4 at a relatively low temperature. In this particular method, $FePO_4{\cdot}2H_2O$ is used as iron and phosphorus precursor, while KBH_4 is employed as a reducing agent. The Fe_2P nanoparticles obtained manifest high discharge capacities and good cycling stability when evaluated as anode materials for nickel-based rechargeable batteries.

2. Experimental

2.1. Preparation of Fe_2P nanoparticles

In a typical procedure, 0.467 g $FePO_4{\cdot}2H_2O$ was homogeneously mixed with 0.200 g KBH_4 in a carnelian mortar. Then, the mixture was heated at 520 °C for 0.5 h and cooled to room temperature under a flow of Ar (99.999%). The solids obtained were washed with water and absolute ethyl alcohol three times, respectively, and then dried in vacuum at 80 °C for 12 h.

2.2. Structural and morphological characterization

Crystalline structure of Fe_2P nanoparticles was determined by X-ray powder diffraction (XRD, Rigaku D/Max-2500 with Cu Kα radiation) and refined by GSAS program [21]. The morphologies were studied by scanning electron microscopy (SEM, SUPRA 55VP Field Emission) and transmission electron microscopy (TEM, Philips Tecnai G2 F20). Elemental composition was evaluated energy dispersive X-ray spectrometer (EDX, EDAX Genesis Apollo X). Electronic states were investigated by X-ray photoelectron spectroscopy (XPS, PHI 5000 VersaProbe). Thermogravimetric analysis (TG) was carried out on an STA-409PC instrument under N_2 (99.999%) atmosphere at a heating rate of 5 °C min^{-1}.

2.3. Electrochemical measurements

For electrochemical measurements, the Fe_2P nanoparticle electrodes were constructed through mixing the products with carbonyl nickel powders in a weight ratio of 1:3. The powder mixtures were pressed under 30 MPa pressure into a small pellet of 10 mm in diameter. Then, the electrodes were conducted in a three compartment cell using an LAND battery test instrument (CT2001A). NiOOH/$Ni(OH)_2$ and Hg/HgO were used as the counter electrode and the reference electrode, respectively. The electrolyte was a 6 M KOH aqueous solution. Charge–discharge cycle tests were carried out at a charge current of 200 mA g^{-1} and a discharge current of 100 mA g^{-1}. The cut-off voltage for discharge test was −0.5 V (vs. Hg/HgO). The testing interval between charge and discharge was 5 min. Zahner IM6e electrochemical workstation was used for cyclic voltammetry (CV) at the rate of 0.2 mV s^{-1} from −1.2 V to −0.2 V (vs. Hg/HgO). All the experiments were conducted at room temperature.

3. Results and discussion

3.1. Material characterization

Fig. 1 shows the representative refinement of XRD patterns of the obtained Fe_2P. The sharp diffraction peaks with high intensity and resolution indicate a high degree of crystallization of the sample. All the diffraction peaks can be well indexed to a hexagonal Fe_2P (space group *P-62m*, JCPDS no. 88-1803) as schematized inset of Fig. 1. No peak from other phases such as crystalline Fe, Fe_3P, or FeP has been detected in the samples, revealing that the Fe_2P obtained is of high purity. The lattice parameters $a = b = 5.880$ Å, $c = 3.449$ Å from the diffraction pattern are in good agreement with literature values for hexagonal Fe_2P. Furthermore, the refined patterns fit the observed data points very well, further confirming the pure phase of Fe_2P.

Fig. 2a shows the SEM image of hexagonal Fe_2P. There are large numbers of particles in irregular shapes. The composition of the obtained Fe_2P was determined by EDX and shown in Fig. 2b. The sample is mainly made up of Fe and P. The molar ratio of Fe to P is about 2:1, which is consistent with the stoichiometric ratio of Fe_2P. Further insight into the structure of hexagonal Fe_2P was confirmed by low- and high-magnification TEM. The obtained Fe_2P generally shows ellipsoidal morphology with diameters of several tens to several hundreds of nanometers, as shown in Fig. 2c. The HRTEM image in Fig. 2d clearly reveals spacings of 0.293 nm and 0.508 nm, which match well with the separations between the neighboring lattices of the (110) and (100) planes of hexagonal Fe_2P, respectively.

The bonding characteristics of the Fe_2P nanoparticles were captured by XPS, where the standard C_{1s} peak was used as a reference for correcting the shifts. The results are shown in Fig. 3. In Fig. 3a, two peaks are observed at 723.2 and 719.8 eV in the $Fe_{2p1/2}$ level, while two peaks accordingly occurs at 709.7 and 706.6 eV in

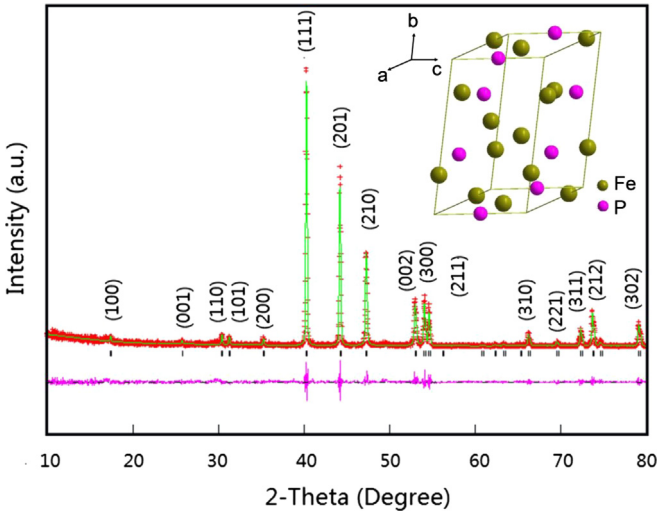

Fig. 1. X-ray diffraction profile of Fe_2P sample: observed (red points), calculated (green line), and difference (bottom pink line). Vertical bars below the patterns show the positions of all possible reflection peaks. The hkl labels are placed according to the reflection position. The inset shows the schematic structures of hexagonal Fe_2P. (For interpretation of the references to colour in this figure legend, the reader is referred to the web version of this article.)

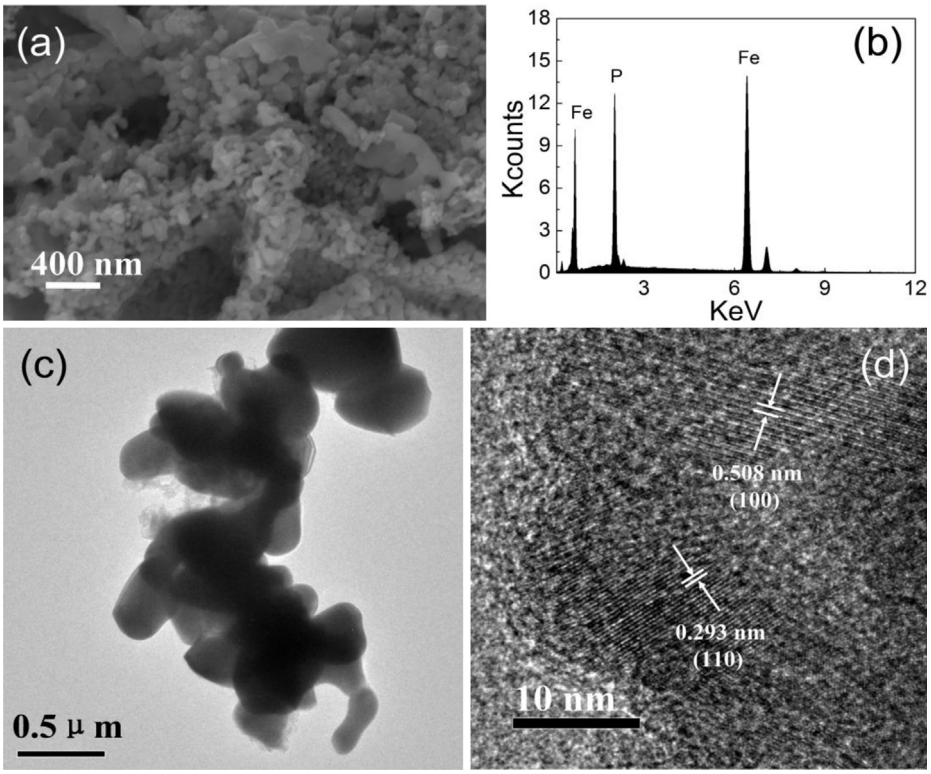

Fig. 2. (a) SEM image and (b) corresponding EDX spectra of as-prepared Fe_2P nanoparticles; (c) TEM and (d) HRTEM images of as-prepared Fe_2P nanoparticles.

the $Fe_{2p3/2}$ level, indicating that Fe exists in both elemental and oxidized states. In Fig. 3b, two peaks are located at 133.0 and 128.9 eV in the P_{2p} level, which are attributed to the elemental and oxidized P. As oxidized Fe and P are not detected in the XRD pattern, thus there may be small amount of them on the surface of Fe_2P nanoparticles. Wu et al. [17] investigated the electrochemical behaviors of FeB alloy, and found that small amount of B_2O_3 on the surface of the FeB alloy would form a protective layer and prevent further oxidation of the FeB alloy. Therefore, these oxidized Fe and P are possibly beneficial for improving the cycling performance of Fe_2P nanoparticles.

3.2. Influences of experimental parameters on the composition of the products

In order to understand the effects of experimental parameters on the composition of the products, a series of studies were carried out. Fig. 4a shows the TG profiles of KBH_4, $FePO_4{\cdot}2H_2O$ and their mixture, respectively. There is about 20% weight loss before 400 °C for $FePO_4{\cdot}2H_2O$, which is attributed to the dehydration of crystal water. No apparent weight loss is observed between 30 °C and 400 °C for KBH_4. The TG curve of the mixture before 400 °C is similar to that of $FePO_4{\cdot}2H_2O$, thus the weight loss of the mixture is possibly generated from the dehydration of $FePO_4{\cdot}2H_2O$. Furthermore, there is a noticeable weight loss occurred between 500 °C and 550 °C for the mixture, which is due to the reduction of $FePO_4$ with KBH_4. After 550 °C, the mass of mixture does not change, indicating the end of reaction between $FePO_4{\cdot}2H_2O$ and KBH_4.

Further insight into the influences of temperatures on the composition of the products were studies by calcining the mixture at 520 °C, 550 °C and 600 °C for 0.5 h, respectively, where the mass ratio of $FePO_4{\cdot}2H_2O$ to KBH_4 was fixed at 0.467:0.2. Fig. 4b shows the XRD patterns of the rinsed products at different temperatures. Pure Fe_2P can be obtained at all the three temperatures, indicating

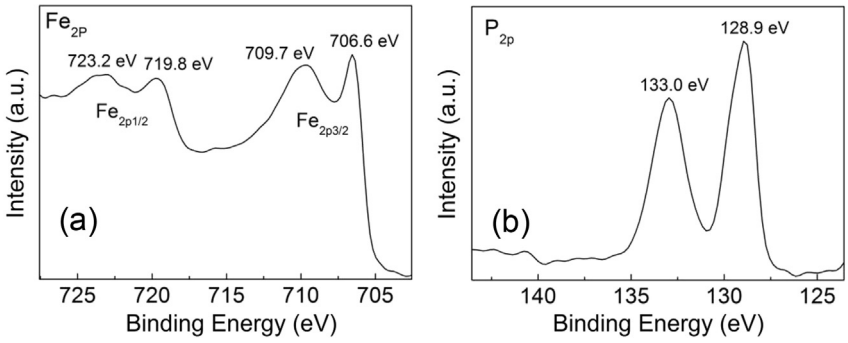

Fig. 3. XPS spectra of (a) Fe_{2p} and (b) P_{2p} for Fe_2P obtained.

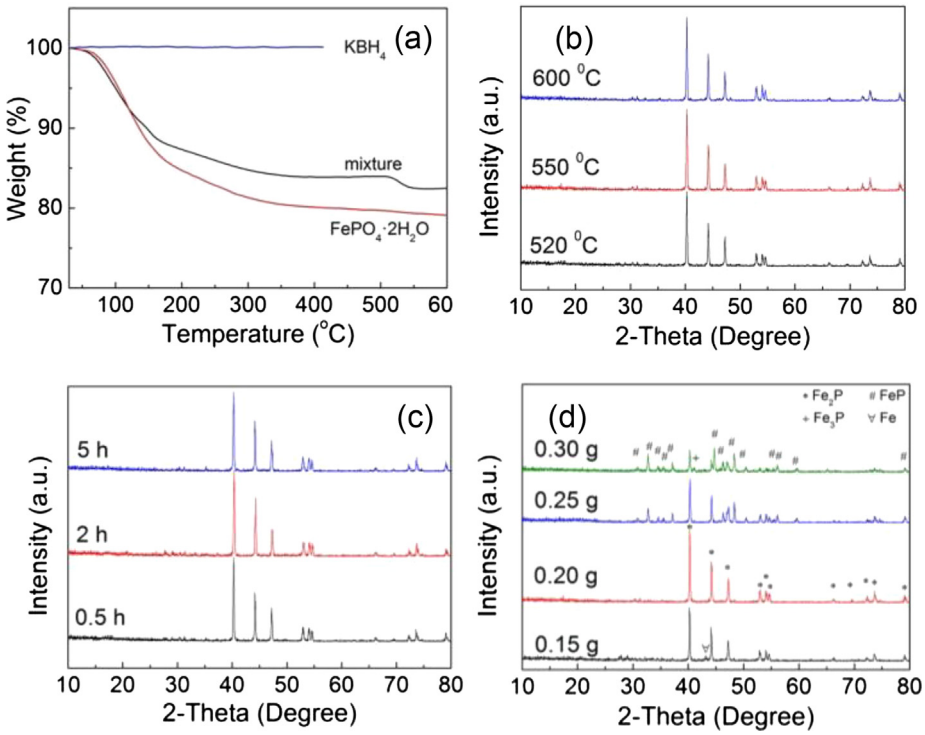

Fig. 4. (a) TG profile generated by heating KBH_4, $FePO_4 \cdot 2H_2O$ and their mixture. (b) XRD patterns of the rinsed products at different temperatures for 0.5 h (The mass ratio of $FePO_4 \cdot 2H_2O$ to KBH_4 is 0.467:0.2). (c) XRD patterns of the rinsed products at 520 °C for different time (The mass ratio of $FePO_4 \cdot 2H_2O$ to KBH_4 is 0.467:0.2). (d) XRD patterns of the rinsed products obtained from the different mass ratios of reactants at 520 °C for 0.5 h.

that the temperature has few effects on the composition of the products when it reaches the lowest value of the solid state reaction between $FePO_4 \cdot 2H_2O$ and KBH_4. This is consistent with the TG results.

The influences of heating time on the composition of the products were also evaluated and shown in Fig. 4c. When the calcination time is increased from 0.5 to 5 h, the final products have no significant difference, indicating that the solid state reaction between $FePO_4 \cdot 2H_2O$ and KBH_4 is very fast. Thus, the heating time does not generally affect the composition of the products.

Fig. 4d shows the XRD patterns of the rinsed products obtained from the different mass ratios of reactants at 520 °C for 0.5 h. It can be seen that the mass ratio of the reactants has an important influence on the composition of the products. When the mass of KBH_4 is 0.15 g, the products have small amounts of Fe impurities besides Fe_2P phase. Pure Fe_2P would only be obtained by use of 0.20 g KBH_4. When KBH_4 is increased to 0.25 g, although the main phase of the products is still Fe_2P, considerable amounts of FeP are also detected. When KBH_4 is further increased to 0.30 g, the content of Fe_2P is decreased while that of FeP is increased. In addition, small amounts of Fe_3P are observed under this condition. According to these results, it seems that Fe would be produced prior to P in the reduction process of $FePO_4$ with KBH_4. The generated Fe and P are combined to form different kinds of Fe–P compounds. The mass of KBH_4 mainly determines the amount of P, and finally affects the compositions of the products. Therefore, this is the key factor of the solid state reaction. It is worth noting that we have tried to transform the mass ratios of $FePO_4 \cdot 2H_2O$ to KBH_4 into molar ratios, but the results are non-stoichiometric. Therefore, the exact solid state reaction mechanism of $FePO_4 \cdot 2H_2O$ and KBH_4 mixture is not very clear. Further studies are still on the way.

3.3. Electrochemical properties

Fig. 5a shows the cycling performance of Fe_2P nanoparticle electrode at a current rate of 100 mA g^{-1}. The initial discharge capacity of 109 mAh g^{-1} is relatively low. During the following 44 cycles, the discharge capacity keeps increasing. The maximum discharge capacity of 413 mAh g^{-1} is obtained in the 45th cycle. Then, Fe_2P nanoparticle electrode exhibits excellent cyclic capacity retention. Even after 100 cycles, a reversible discharge capacity of 396 mAh g^{-1} can still be retained.

To understand the activation process of Fe_2P nanoparticle electrode, the charge and discharge curves at different cycles are shown in Fig. 5b. In the first cycle, there is no apparent charge plateau but a discharge plateau at −0.65 V. In the second cycle, a charge plateau appears at −0.92 V, and two discharge plateaus are observed at −0.65 V and −0.87 V, respectively. The lengths of these three voltage plateaus are continuously increased in the next 43 cycles. It seems that more and more active materials participate in the electrochemical reaction during the activation process. This is very similar to the reported Co–P and Co_2P electrodes [15,16]. Actually, the effects of several nonmetal elements such as B, P and S on the electrochemical properties of Co-based electrodes have previous been reported [16,22,23]. These nonmetal elements will dissolved in KOH solution during electrochemical reactions to generate new interspaces in electrodes. Thus, more and more active materials will contact with electrolyte, which is helpful for improving the electrochemical performance of the electrodes. However, the dissolution of P in KOH solution is relatively slow [15,16]. Therefore, a long time activation process is usually needed. A similar mechanism may be deduced for Fe_2P nanoparticle electrode.

Fig. 5c shows the typical CV curve of Fe_2P nanoparticle electrode in 6 M KOH aqueous solution. A remarkable reduction peak

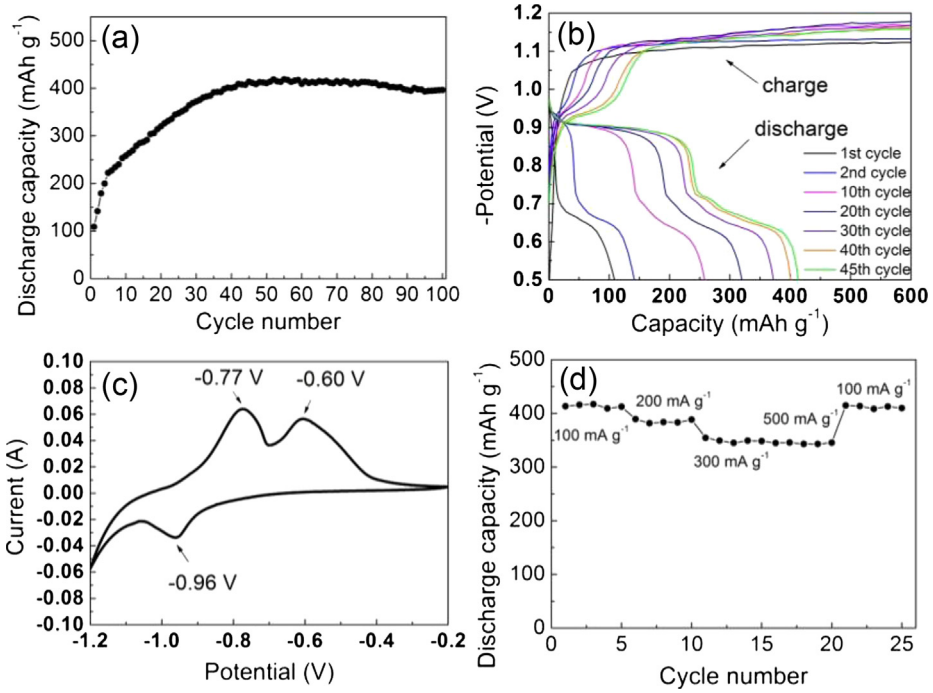

Fig. 5. (a) Cycling performance of Fe_2P nanoparticle electrode at 100 mA g^{-1}. (b) Charge/discharge curves of Fe_2P nanoparticle electrode at a charge current of 200 mA g^{-1} and a discharge current of 100 mA g^{-1}. (c) Typical CV curve of Fe_2P nanoparticle electrode at a scan rate of 0.2 mV s^{-1}. (d) Rate performance of Fe_2P nanoparticle electrode charged at 200 mA g^{-1} and discharged at various rates.

appears at −0.96 V which is related to the charge plateau at −0.92 V. Accordingly, two strong oxidation peaks arise at −0.77 V and −0.60 V, which correspond to the two discharge plateaus at −0.65 V and −0.87 V, respectively. The shape of the CV curve of Fe_2P nanoparticle electrode is similar to that of reported FeB alloy [17]. Further studies on the exact electrochemical reaction mechanism are still underway.

As the rate capability is also critical for practical applications, it was evaluated at various current densities from 100 to 500 mA g^{-1} for Fe_2P nanoparticle electrode, as presented in Fig. 5d. The discharge capacities of 413, 385 and 345, 343 mAh g^{-1} can be obtained at rates of 100, 200, 300 and 500 mA g^{-1}, respectively, showing attractive rate performance. Furthermore, the discharge capacity can still be recovered to almost the same value by using a small density of 100 mA g^{-1} after deep cycling at a high current density of 500 mA g^{-1}, indicating that Fe_2P nanoparticles have great potential as a high-rate anode material for nickel-based rechargeable batteries.

4. Conclusion

In summary, Fe_2P nanoparticles have been successfully prepared *via* the solid state reaction between $FePO_4 \cdot 2H_2O$ and KBH_4, and electrochemically used as anode materials for nickel-based rechargeable batteries. The mass ratio of $FePO_4 \cdot 2H_2O$ to KBH_4 has a decisive influence on the composition of the products. The reversible discharge capacity of Fe_2P nanoparticle electrode is 413 mAh g^{-1} at a discharge current of 100 mA g^{-1}. Moreover, Fe_2P nanoparticle electrode exhibits attractive rate capability. Discharge capacities of 385, 345 and 343 mAh g^{-1} are achieved at 200, 300 and 500 mA g^{-1}, respectively. To the best of our knowledge, the synthesis of Fe_2P nanoparticles employing such a solid state reaction and the evaluation of them as anode materials for nickel-based rechargeable batteries are reported for the first time. It shall be possible to extend this special method for preparing other transition metal phosphides such as Co_2P, and Ni_2P.

Acknowledgment

This work was financially supported by MOST Projects (2011CB935900, 2012AA051901), NSFC (51071087, 21231005), 111 Project (B12015), Tianjin Sci & Tech Project (10SYSYJC27600), Nature Science Foundation of Tianjin (11JCYBJC07700), Research Fund for the Doctoral Program of Higher Education of China (20120031110001), the 863 Program (2012AA111401) and the Natural Science Foundation of Jiangsu Province (BK2012293, BK20130482).

References

[1] K. Vijayamohanan, T.S. Balasubramanian, A.K. Shukla, J. Power Sources 34 (1991) 269–285.
[2] K. Micka, Z. Zabransky, J. Power Sources 19 (1987) 315–323.
[3] M.E. Unates, E. Folquer, J.R. Vilche, A.J. Arvia, J. Electrochem. Soc. 139 (1992) 2697–2704.
[4] E.J. Casey, A.R. Dubois, P.E. Lake, W.J. Moroz, J. Electrochem. Soc. 112 (1965) 371–383.
[5] X.Y. Xiong, H. Vander Poorten, M. Crappe, Electrochim. Acta 41 (1996) 1267–1275.
[6] D.J. Cuscueta, H.L. Corso, A. Arenillas, P.S. Martinez, A.A. Ghilarducci, H.R. Salva, Int. J. Hydrogen Energy 37 (2012) 14978–14982.
[7] A. Etiemble, S. Rousselot, W. Guo, H. Idrissi, L. Roué, Int. J. Hydrogen Energy 38 (2013) 7169–7177.
[8] W.H. Zhu, Y. Zhu, Z. Davis, B.J. Tatarchuk, Appl. Energy 106 (2013) 307–313.
[9] F.C. Ruiz, P.S. Martínez, E.B. Castro, R. Humana, H.A. Peretti, A. Visintin, Int. J. Hydrogen Energy 38 (2013) 240–245.
[10] J. Jindra, J. Power Sources 66 (1997) 15–25.
[11] Y.F. Yuan, J.P. Tu, H.M. Wu, Y.Z. Yang, D.Q. Shi, X.B. Zhao, Electrochim. Acta 51 (2006) 3632–3636.
[12] M. Mitov, A. Popov, I. Dragieva, J. Appl. Electrochem. 29 (1999) 59–64.
[13] Y.D. Wang, X.P. Ai, Y.L. Cao, H.X. Yang, Electrochem. Commun. 6 (2004) 780–784.
[14] Y.D. Wang, X.P. Ai, H.X. Yang, Chem. Mater. 16 (2004) 5194–5197.

[15] Y.L. Cao, W.C. Zhou, X.Y. Li, X.P. Ai, X.P. Gao, H.X. Yang, Electrochim. Acta 51 (2006) 4285–4290.
[16] W.X. Peng, L.F. Jiao, Q.N. Huan, L. Li, J.Q. Yang, Q.Q. Zhao, Q.H. Wang, H.M. Du, G. Liu, Y.C. Si, Y.J. Wang, H.T. Yuan, J. Alloys Compd. 511 (2012) 198–201.
[17] Y. Bai, C. Wu, F. Wu, L.X. Yang, B.R. Wu, Electrochem. Commun. 11 (2009) 145.
[18] X.Q. Wang, P. Clark, S.T. Oyama, J. Catal. 208 (2002) 321–331.
[19] Y.L. Gu, F. Guo, Y.T. Qian, H.G. Zheng, Z.P. Yang, Mater. Res. Bull. 37 (2002) 1101–1105.
[20] H.D. She, Y.Z. Chen, R.T. Wen, K. Zhang, G.H. Yue, D.L. Peng, Nanoscale Res. Lett. 5 (2010) 786–790.
[21] B.H. Toby, J. Appl. Cryst. 34 (2001) 210–213.
[22] Y.P. Wang, L. Li, Y.J. Wang, D.W. Song, G. Liu, Y. Han, L.F. Jiao, H.T. Yuan, J. Power Sources 196 (2011) 5731–5736.
[23] D.W. Song, Y.J. Wang, Q.H. Wang, Y.P. Wang, L.F. Jiao, H.T. Yuan, J. Power Sources 195 (2010) 7115–7119.